

# Large-basis *ab initio* no-core shell model and its application to $^{12}\text{C}$

P. Navrátil,<sup>1,2,\*</sup> J. P. Vary,<sup>3</sup> and B. R. Barrett<sup>1</sup>

<sup>1</sup>*Department of Physics, University of Arizona, Tucson, Arizona 85721*

<sup>2</sup>*Nuclear Physics Institute, Academy of Sciences of the Czech Republic, 250 68 Rež near Prague, Czech Republic*

<sup>3</sup>*Department of Physics and Astronomy, and International Institute of Theoretical and Applied Physics, Iowa State University, Ames, Iowa 50011*

(Received 16 August 2000; published 10 October 2000)

We present the framework for the *ab initio* no-core nuclear shell model and apply it to obtain properties of  $^{12}\text{C}$ . We derive two-body effective interactions microscopically for specific model spaces from the realistic CD-Bonn and the Argonne V8' nucleon-nucleon ( $NN$ ) potentials. We then evaluate binding energies, excitation spectra, radii, and electromagnetic transitions in the  $0\hbar\Omega$ ,  $2\hbar\Omega$ , and  $4\hbar\Omega$  model spaces for the positive-parity states and the  $1\hbar\Omega$ ,  $3\hbar\Omega$ , and  $5\hbar\Omega$  model spaces for the negative-parity states. Dependence on the model-space size, on the harmonic-oscillator frequency, and on the type of the  $NN$  potential, used for the effective interaction derivation, are studied. In addition, electromagnetic and weak neutral elastic charge form factors are calculated in the impulse approximation. Sensitivity of the form-factor ratios to the strangeness one-body form-factor parameters and to the influence of isospin-symmetry violation is evaluated and discussed. Agreement between theory and experiment is favorable for many observables, while others require yet larger model spaces and/or three-body forces. The limitations of the present results are easily understood by virtue of the trends established and previous phenomenological results.

PACS number(s): 21.60.Cs, 21.30.Fe, 24.10.Cn, 27.20.+n

## I. INTRODUCTION

While various methods have been developed to solve exactly the three- and four-nucleon systems with realistic interactions [1–4], few approaches are applicable for nuclei with more than four nucleons at this time. Apart from the coupled cluster method [5] applied typically to closed-shell and near-closed shell nuclei, the Green's-function Monte Carlo method is the only approach for which exact solutions of systems with  $A \leq 8$  interacting by realistic potentials have been obtained [4].

We evaluate the properties of more complex nuclei, treated as systems of nucleons interacting by realistic nucleon-nucleon ( $NN$ ) interactions, with our method for the no-core shell model [6–8]. At present, we formulate [9–11] the no-core shell model as a unitary transformation of the  $A$ -body Hamiltonian followed by a two-body cluster approximation. That is, the unitary transformation is determined from a model-space decoupling condition, which is fulfilled on the two-body cluster level. The resulting transformed Hamiltonian consists of a one-body term and the two-body effective interaction. The calculation is performed in the harmonic-oscillator (HO) basis, and due to the cluster approximation, we acquire dependence on two parameters. One parameter determines the model-space size and the other is the HO frequency. The method becomes independent of the HO frequency and is convergent to the exact result with increasing model-space size. The trend towards parameter-free results is a specific focus of this investigation.

We emphasize that once the original many-body Hamiltonian is defined, our *ab initio* no-core nuclear shell model

provides a subset of the exact solutions. Our *sole* approximation will be to treat our theoretically derived effective operators at the two-body-cluster level. This single approximation results in the dependencies on the model-space size and the HO frequency. For realistic nuclear Hamiltonians with  $NN$  interactions fitting available data, we show that the dependencies on the model-space size and the HO frequency weaken considerably with the increasing model-space size, indicating smaller changes would arise by proceeding to higher-body clusters.

We have shown that the no-core shell-model approach can be consistently applied to solve the three-nucleon as well as the four-nucleon bound-state problem [9]. In particular, we were able to find the ground-state solution for  $^4\text{He}$  interacting by the CD-Bonn  $NN$  potential [10]. An equivalent formulation of this approach that results in a successful description of  $A = 3$  and  $A = 4$  systems is applied in the present paper to a significantly more complex system,  $^{12}\text{C}$ .

There are important physics motivations for investigating  $^{12}\text{C}$ . The  $^{12}\text{C}$  nucleus plays an important role in neutrino studies, as it is an ingredient of the neutrino liquid-scintillator detectors. Theoretical description and understanding of the neutrino interactions with  $^{12}\text{C}$  is, therefore, crucial [12,13].

There has been considerable interest recently in parity-violating electron scattering from protons and light nuclei. One of the main reasons for this has been to investigate the strangeness content of the nucleon [14,15]. The  $(J^\pi, T) = (0^+, 0)$  targets, like  $^{12}\text{C}$ , are of particular interest because they support only the isoscalar matrix element of the Coulomb operator.

In order to describe theoretically the electron scattering or other electroweak processes one needs, first, the appropriate scattering operators. The scattering operators typically consist of the one-body part used in the impulse approximation

\*Present address: University of California, Lawrence Livermore National Laboratory, P.O. Box 808, Livermore, CA 94551.

calculations and the two-body part given by the meson-exchange currents (MEC's). The computation of such operators has been explored thoroughly in the literature, e.g., in Refs. [16,17]. Second, reliable nuclear many-body wave functions are needed. Our work concentrates on this second aspect.

In principle, one also needs many-body effective operators, which are obtainable within our framework. However, we will mostly neglect these effective operator contributions at present and, instead, work in the largest feasible model space, so as to minimize these neglected contributions.

The no-core shell-model calculations are performed in such a way that the center-of-mass (c.m.) motion and the internal motion are completely factorized. Translational invariance is preserved and, for example, the form factors then depend only on the relative coordinates.

In addition to the physics motivations,  $^{12}\text{C}$  provides a challenging technological application of our no-core shell-model approach. The dimensions are larger than 6 000 000 for a  $5\hbar\Omega$  model space in the  $m$  scheme. Indeed, there have been multi- $\hbar\Omega$  shell-model studies of  $^{12}\text{C}$  in the past [18–20], but unlike our approach, phenomenological effective interactions and smaller model spaces were used in those calculations.

In Sec. II, we discuss our no-core shell-model formulation, i.e., the Hamiltonian and effective interaction framework together with a test for the  $A=3$  system. Results for the  $A=12$  system interacting by the CD-Bonn and the Argonne V8'  $NN$  potentials are given in Sec. III. We discuss the binding energies, excitation spectra, electromagnetic (EM) properties as well as EM charge and strangeness form factors. In Sec. IV, we present concluding remarks.

## II. NO-CORE SHELL-MODEL APPROACH

### A. Hamiltonian

In the no-core shell-model approach we start from the purely intrinsic Hamiltonian for the  $A$ -nucleon system, i.e.,

$$H_A = T_{\text{rel}} + \mathcal{V} = \frac{1}{A} \sum_{i < j} \frac{(\vec{p}_i - \vec{p}_j)^2}{2m} + \sum_{i < j=1}^A V_N(\vec{r}_i - \vec{r}_j), \quad (1)$$

where  $m$  is the nucleon mass and  $V_N(\vec{r}_i - \vec{r}_j)$ , is the  $NN$  interaction. It is purely a two-body operator without a phenomenological single-particle potential. At present, we omit three-body potentials, which are known from other works [4] to be necessary for high-quality fits to data. This work is intended to establish a baseline of results at the pure two-body interaction level.

We can use both coordinate-space dependent  $NN$  potentials, such as the Argonne potentials [4] as well as momentum-space dependent  $NN$  potentials, such as the CD-Bonn [21]. In the next step we modify the Hamiltonian (1) by adding to it the center-of-mass HO Hamiltonian  $H_{\text{c.m.}} = T_{\text{c.m.}} + U_{\text{c.m.}}$ , where  $U_{\text{c.m.}} = \frac{1}{2}Am\Omega^2\vec{R}^2$ ,  $\vec{R} = (1/A)\sum_{i=1}^A\vec{r}_i$ . This HO CM Hamiltonian will be subtracted again in the final many-body calculation so there is no net influence on intrinsic properties of the many-body system. In fact, in the

full space such a potential has no influence on the intrinsic properties at all. However, this added and/or subtracted potential facilitates the use of the convenient HO basis for evaluating the effective interactions. The modified Hamiltonian, with a pseudodependence on the HO frequency  $\Omega$ , can be cast into the form

$$H_A^\Omega = \sum_{i=1}^A \left[ \frac{\vec{p}_i^2}{2m} + \frac{1}{2}m\Omega^2\vec{r}_i^2 \right] + \sum_{i < j=1}^A \left[ V_N(\vec{r}_i - \vec{r}_j) - \frac{m\Omega^2}{2A}(\vec{r}_i - \vec{r}_j)^2 \right]. \quad (2)$$

Since we solve the many-body problem in a finite HO model space, the realistic nuclear interaction in Eq. (2) will yield pathological results unless we use it to derive a model-space-dependent effective Hamiltonian. In general, for an  $A$ -nucleon system, an  $A$ -body effective interaction is needed. As we discuss in detail in the next subsection, we make a two-body cluster approximation for the effective interaction in the present calculations. Large model spaces are desirable to minimize the role of neglected effects, which a larger cluster would include. In addition, the larger the model space is, generally speaking, the smaller, the neglected renormalization contributions to the effective operators.

As the Hamiltonians  $H_A$  (1) and  $H_A^\Omega$  (2) differ only by a c.m.-dependent term, no dependence on  $\Omega$  should exist for the intrinsic properties of the nucleus. However, because of the two-body-cluster approximation for the effective interaction, a dependence on  $\Omega$  appears in our calculations. This dependence of results on  $\Omega$  and size of the model space provides one gauge of the severity of this approximation. Fortunately, some important observables have significant  $\Omega$  independence and model space independence in our largest model spaces.

### B. Two-body effective interaction and the model space definition

In order to derive the effective interaction, we employ the Lee-Suzuki similarity transformation method [22,23], which yields a Hermitian effective interaction. The approach presented here leads to the same two-body effective interaction as used in our previous papers [9,10].

Let us write the Hamiltonian (2) schematically as

$$H_A^\Omega = \sum_{i=1}^A h_i + \sum_{i < j=1}^A V_{ij}. \quad (3)$$

In the spirit of Da Providencia and Shakin [24] and Lee, Suzuki, and Okamoto [22,23], we introduce a unitary transformation of the Hamiltonian, which is able to accommodate the short-range two-body correlations in a nucleus, by choosing an anti-Hermitian operator  $S$ , such that

$$\mathcal{H} = e^{-S} H_A^\Omega e^S. \quad (4)$$

In our approach,  $S$  is determined by the requirements that  $\mathcal{H}$  and  $H_A^\Omega$  have the same symmetries and eigenspectra over the

subspace  $\mathcal{K}$  of the full Hilbert space. In general, both  $S$  and the transformed Hamiltonian are  $A$ -body operators. Our simplest, nontrivial approximation to  $\mathcal{H}$  is to develop a two-body effective Hamiltonian. The next improvement is to develop a three-body effective Hamiltonian. This approach consists then of an approximation to a particular level of clustering:

$$\mathcal{H} = \mathcal{H}^{(1)} + \mathcal{H}^{(a)}, \quad (5)$$

where the one-body and  $a$ -body ( $a \leq A$ ) pieces are given as

$$\mathcal{H}^{(1)} = \sum_{i=1}^A h_i, \quad (6a)$$

$$\mathcal{H}^{(a)} = \frac{\binom{A}{2}}{\binom{A}{a} \binom{a}{2}} \sum_{i_1 < i_2 < \dots < i_a} \tilde{V}_{i_1 i_2 \dots i_a}, \quad (6b)$$

with

$$\tilde{V}_{i_2 \dots i_a} = e^{-S^{(a)}} H_a^\Omega e^{S^{(a)}} - \sum_{i=1}^a h_i, \quad (7)$$

where  $S^{(a)}$  is an  $a$ -body operator:

$$H_a^\Omega = h_1 + h_2 + h_3 + \dots + h_a + V_a; \quad (8)$$

and

$$V_a = \sum_{i < j}^a V_{ij}. \quad (9)$$

Note that there is no sum over ‘‘ $a$ ’’ in Eq. (5).

In the above equations, it has been assumed that the basis states are eigenstates of the one-body (in our case HO), Hamiltonian  $\sum_{i=1}^A h_i$ .

If the full space is divided into a model space and a  $Q$  space, using the projectors  $P$  and  $Q$  with  $P + Q = 1$ , it is possible to determine the transformation operator  $S_a$  from the decoupling condition

$$Q_a e^{-S^{(a)}} H_a^\Omega e^{S^{(a)}} P_a = 0, \quad (10)$$

and the simultaneous restrictions  $P_a S^{(a)} P_a = Q_a S^{(a)} Q_a = 0$ . Note that  $a$ -nucleon-state projectors ( $P_a, Q_a$ ) appear in Eq. (10). Their definitions follow from the definitions of the  $A$ -nucleon projectors  $P, Q$ . This approach, introduced by Suzuki and Okamoto and referred to as the unitary-model-operator approach [25], has a solution that can be expressed in the following form:

$$S^{(a)} = \text{arctanh}(\omega - \omega^\dagger), \quad (11)$$

with the operator  $\omega$  satisfying  $\omega = Q_a \omega P_a$ . Let us remark that this is the same operator, which solves the equation

$$Q_a e^{-\omega} H_a^\Omega e^{\omega} P_a = 0. \quad (12)$$

Let us also note that  $\bar{H}_{a\text{-eff}} = P_a e^{-S^{(a)}} H_a^\Omega e^{S^{(a)}} P_a$  leads to the relation

$$\begin{aligned} \bar{H}_{a\text{-eff}} &= (P_a + \omega^\dagger \omega)^{-1/2} (P_a + P_a \omega^\dagger Q_a) H_a^\Omega \\ &\quad \times (Q_a \omega P_a + P_a) (P_a + \omega^\dagger \omega)^{-1/2}. \end{aligned} \quad (13)$$

If the eigensolutions of the Hamiltonian  $H_a^\Omega$  are given by  $H_a^\Omega |k\rangle = E_k |k\rangle$ , then the operator  $\omega$  can be determined as

$$\langle \alpha_Q | \omega | \alpha_P \rangle = \sum_{k \in \mathcal{K}} \langle \alpha_Q | k \rangle \langle \tilde{k} | \alpha_P \rangle, \quad (14)$$

where we denote by the tilde the inverted matrix of  $\langle \alpha_P | k \rangle$ , i.e.,  $\sum_{\alpha_P} \langle \tilde{k} | \alpha_P \rangle \langle \alpha_P | k' \rangle = \delta_{k,k'}$  and  $\sum_k \langle \alpha_P' | \tilde{k} \rangle \langle k | \alpha_P \rangle = \delta_{\alpha_P', \alpha_P}$ , for  $k, k' \in \mathcal{K}$ . In relation (14),  $|\alpha_P\rangle$  and  $|\alpha_Q\rangle$  are the model-space and the  $Q$ -space basis states, respectively, and  $\mathcal{K}$  denotes a set of  $d_P$  eigenstates, whose properties are reproduced in the model space, with  $d_P$  equal to the dimension of the model space. Physical and mathematical properties of Eqs. (12) and (14) may be found in Ref. [26].

With the help of the solution for  $\omega$  [Eq. (14)] we obtain a simple expression for the matrix elements of the Hermitian effective Hamiltonian

$$\begin{aligned} \langle \alpha_P | \bar{H}_{a\text{-eff}} | \alpha_P' \rangle &= \sum_{k \in \mathcal{K}} \sum_{\alpha_P''} \sum_{\alpha_P'''} \langle \alpha_P | (P_a + \omega^\dagger \omega)^{-1/2} | \alpha_P'' \rangle \\ &\quad \times \langle \alpha_P'' | \tilde{k} \rangle E_k \langle \tilde{k} | \alpha_P''' \rangle \\ &\quad \times \langle \alpha_P''' | (P_a + \omega^\dagger \omega)^{-1/2} | \alpha_P' \rangle. \end{aligned} \quad (15)$$

For computation of the matrix elements of  $(P_a + \omega^\dagger \omega)^{-1/2}$ , we can use the relation

$$\langle \alpha_P | (P_a + \omega^\dagger \omega)^{-1/2} | \alpha_P' \rangle = \sum_{k \in \mathcal{K}} \langle \alpha_P | \tilde{k} \rangle \langle \tilde{k} | \alpha_P' \rangle. \quad (16)$$

Now, we introduce our present application, in which we take  $a = 2$ . Let us write explicitly the two-nucleon Hamiltonian in the relative and c.m. coordinates, e.g.,

$$\begin{aligned} H_{A=2}^\Omega &= H_{02} + H_{2c.m.} + V_{12} \\ &= \frac{\vec{p}^2}{2m} + \frac{1}{2} m \Omega^2 \vec{r}^2 + H_{2c.m.} + V_N(\sqrt{2}\vec{r}) - \frac{m\Omega^2}{A} \vec{r}^2, \end{aligned} \quad (17)$$

where  $H_{02} + H_{2c.m.} = h_1 + h_2$ ,  $\vec{r} = \sqrt{\frac{1}{2}}(\vec{r}_1 - \vec{r}_2)$  and  $\vec{p} = \sqrt{\frac{1}{2}}(\vec{p}_1 - \vec{p}_2)$ . The two-nucleon problem is then solved in a relative HO basis space with high precision. The c.m. motion of the two nucleons is not affected by the transformation  $S^{(2)}$ . The term  $H_{2c.m.}$  does not contribute to the effective interaction calculation and cancels out as seen in Eq. (7). The  $A$  in Eq. (17) is set to 12 in the present application.

The relative-coordinate two-nucleon HO states used in the calculation are characterized by quantum numbers  $|nlsjt\rangle$  with the radial and orbital HO quantum numbers correspond-

ing to coordinate  $\vec{r}$  and momentum  $\vec{p}$ , respectively. Typically, we solve the two-nucleon Hamiltonian (17) for all two-nucleon channels up to  $j=6$ . For the channels with higher  $j$  we take  $V_N$  to be zero. Thus, only the relative kinetic term contributes in such channels in the many-nucleon calculation.

The model space  $P_2$  is defined by the maximal number of allowed HO excitations of the  $A$ -nucleon system  $N_{\text{totmax}}$  from the condition  $2n+l \leq N_{\text{totmax}} - N_{\text{spsmin}}$ , where  $N_{\text{spsmin}}$  denotes the minimal possible value of the HO quanta of the spectators, i.e., nucleons not affected by the interaction process. For  $^{12}\text{C}$ ,  $N_{\text{spsmin}}=6$  as there are eight nucleons in the  $0p$  shell in the unperturbed ground-state configuration and, e.g.,  $N_{\text{totmax}}=N_{\text{spsmin}}+2+N_{\text{max}}$ , where  $N_{\text{max}}$  represents the maximum HO quanta of the many-body excitation above the unperturbed ground-state configuration. For  $^{12}\text{C}$ ,  $N_{\text{totmax}}=12$  for a “ $4\hbar\Omega$ ” calculation. It is possible to include the effects of configurations, in which the spectator nucleons are excited, in the form of the so-called multivalued two-body interaction [7]. Doing this improved the excited-state spectrum outside the  $0\hbar\Omega$  part of the model space at the expense of introducing a variable parameter to correct for overbinding the nucleus. In the present calculations we have no variable parameters and, hence, prefer to perform our calculations with the single, energy-independent two-body effective interaction, defined above.

At this stage, the many-body  $P$  space is defined by either  $N_{\text{totmax}}$  or  $N_{\text{max}}$  which then controls the configurations (Slater determinants) of single-particle states included in the model space. However, only a nonredundant subset of these states are needed to span the translationally invariant  $A$ -nucleon  $P$  space. We isolate this subset by adding a term  $\Lambda(H_{\text{c.m.}} - \frac{3}{2}\hbar\Omega)$  to the effective Hamiltonian with  $\Lambda \geq 10$ . This procedure moves the states with excited c.m. motion correspondingly higher in the calculations and away from the physically relevant states all of which have a (passive)  $0S$  state of c.m. motion. It is, therefore, proper to take this combined process of defining  $N_{\text{totmax}}$  or  $N_{\text{max}}$  along with the “projection” of the physically relevant subset of states (with  $0S$  c.m. motion) as the definition of our many-body  $P$  space. The two-nucleon effective interaction is solved for a relative coordinate  $P_2$  space consistent with this definition of the many-body  $P$  space.

In order to construct the operator  $\omega$  [Eq. (14)] we need to select the set of eigenvectors  $\mathcal{K}$ . In the present application we select the lowest states obtained in each two-body channel. It turns out that these states also have the largest overlap with the model space for the range of  $\hbar\Omega$  we investigate and the  $P$  spaces we select. Their number is given by the number of basis states satisfying  $2n+l \leq N_{\text{totmax}} - N_{\text{spsmin}}$ .

Finally, the two-body effective interaction is determined from the two-nucleon effective Hamiltonian, obtained from Eq. (15), as  $V_{2\text{eff}} = \tilde{V}_{12} = \bar{H}_{2\text{eff}} - h_1 - h_2$ . Apart from being a function of the nucleon number  $A$ ,  $V_{2\text{eff}}$  depends on the HO frequency  $\Omega$  and on the parameter  $N_{\text{totmax}}$ , defining the model space. It has the important property that  $V_{2\text{eff}} \rightarrow V_{12}$  for  $N_{\text{totmax}} \rightarrow \infty$ , following from the fact that  $\omega \rightarrow 0$  for  $P \rightarrow 1$ . We note that  $\mathcal{H}^{(1)} + \mathcal{H}^{(2)} - H_{\text{c.m.}}$  is translationally invariant.

A significant consequence of preserving translational invariance is the factorization of each of our wave functions into a product of a c.m.  $\frac{3}{2}\hbar\Omega$  wave function and a wave function corresponding to the internal motion. Due to this property, it is straightforward to remove c.m. effects exactly from all observables. This feature distinguishes our approach from most phenomenological shell-model studies that involve two or more major HO shells.

We note that the introduction of a mean-field potential, in our case the HO potential [see Eqs. (2),(17)] and its removal in a later phase, is crucial for the reduction of the contributions from the higher-order clusters. It guarantees a large overlap of the model space with the bound and quasibound eigenstates of the Hamiltonian (17) that are used for the effective-interaction calculation.

As discussed previously, we could also perform our calculations at the three-body-cluster level for  $^{12}\text{C}$ , instead of at the two-body-cluster level. We have performed such three-body-cluster level calculations for the  $A=4$  system [9,10]. We learned from these studies as well as from the  $A=3$  results presented in the Sec. II D that the ground-state energy changes by about 10% in going from the two-body cluster to the three-body cluster. These results hold for similar model spaces, as those that we employ in the present calculation for  $^{12}\text{C}$ , when a physically reasonable HO frequency is chosen.

We may actually try to estimate the range of changes that will occur when we improve our approach from a two-body cluster approximation to a three-body cluster approximation for nuclei beyond  $A=4$ .

We base our estimate on results from  $A=3$  and  $A=4$  with two-body cluster calculations (see Ref. [10]), since exact answers are known from other methods.

In Table I we present the change in binding energy per nucleon  $[\Delta(E/A)]$  divided by change in  $\hbar\Omega$   $[\Delta(\hbar\Omega)]$  at fixed  $N_{\text{max}}$  and located around the preferred  $\hbar\Omega$  for CD-Bonn in  $A=3$  and  $A=4$ . We took the preferred  $\hbar\Omega = 28$  MeV in  $A=3$  and the preferred  $\hbar\Omega = 40$  MeV in  $A=4$  since these results are least dependent on  $N_{\text{max}}$ .

Working with the  $N_{\text{max}}=4-12$  results in  $A=3$  and 4, we observe that the slope  $[\Delta(E/A)]/[\Delta(\hbar\Omega)]$  at fixed  $N_{\text{max}}$  and at the preferred  $\hbar\Omega$  exhibits roughly an “ $A-1$ ” effect. That is, the slope increases with  $A$  roughly as  $A-1$  especially for the higher values of  $N_{\text{max}}$  (which have lower coefficients for the effect). This would translate into an  $A(A-1)$  effect in the total binding energy and leads us to conclude that the dominant binding energy correction is following a two-body cluster scaling behavior rather than a three-body cluster scaling [which would follow  $A(A-1)(A-2)$ ].

This is quite encouraging and suggests that the difference between two-body and three-body cluster results is reasonably small when working around the preferred  $\hbar\Omega$  for  $^{12}\text{C}$ .

This conclusion of an estimated suppression in the changes arising from the extension of our method to three-body clusters is tied to the fact that we have a preferred  $\hbar\Omega$  where there is an approximate model space independence and convergence to the exact result is optimal. Having such a preferred  $\hbar\Omega$  minimizes the “leading” correction [the  $A(A-1)(A-2)$  effect in this case] leaving us with the subdominant correction [the  $A(A-1)$  effect].

TABLE I. The change in binding energy per nucleon,  $\Delta(E/A)$ , divided by change in  $\hbar\Omega$ ,  $\Delta(\hbar\Omega)$ , at fixed  $N_{\max}$  and located around the preferred  $\hbar\Omega$  for CD-Bonn in  $A=3$  and  $A=4$ . The differences were obtained using the  $\hbar\Omega$  results which bracket the ‘‘preferred  $\hbar\Omega$ ’’ results. The ground-state energy results for  ${}^3\text{H}$  correspond to those shown in Fig. 1. The  ${}^4\text{He}$  results are taken from Ref. [10].

${}^3\text{H}$					
$\hbar\Omega = 22 \text{ MeV}$					
$N_{\max}$	4	6	8	10	12
$E_{\text{gs}} \text{ (MeV)}$	-8.458	-8.355	-8.258	-8.219	-8.151
preferred $\hbar\Omega = 28 \text{ MeV}$					
$N_{\max}$	4	6	8	10	12
$E_{\text{gs}} \text{ (MeV)}$	-7.760	-7.890	-7.902	-7.977	-7.970
$\hbar\Omega = 32 \text{ MeV}$					
$N_{\max}$	4	6	8	10	12
$E_{\text{gs}} \text{ (MeV)}$	-7.206	-7.519	-7.648	-7.791	-7.843
$\frac{\Delta(E/A)}{\Delta(\hbar\Omega)}$	0.0417	0.0279	0.0203	0.0143	0.0103
${}^4\text{He}$					
$\hbar\Omega = 37 \text{ MeV}$					
$N_{\max}$	4	6	8	10	12
$E_{\text{gs}} \text{ (MeV)}$	-27.062	-26.768	-26.533	-26.440	-26.358
preferred $\hbar\Omega = 40 \text{ MeV}$					
$N_{\max}$	4	6	8	10	12
$E_{\text{gs}} \text{ (MeV)}$	-26.156	-26.207	-26.181	-26.181	-26.189
$\hbar\Omega = 43 \text{ MeV}$					
$N_{\max}$	4	6	8	10	12
$E_{\text{gs}} \text{ (MeV)}$	-25.193	-25.599	-25.808	-25.907	-26.017
$\frac{\Delta(E/A)}{\Delta(\hbar\Omega)}$	0.0779	0.0487	0.0301	0.0222	0.0143
$(A=4)/(A=3)$	1.86	1.75	1.48	1.55	1.39

### C. Renormalization of other operators

It is straightforward to formulate the procedure for a renormalization of general operators within our formalism. A two-body correction to a one-body operator  $\hat{O} = \sum_{i=1}^A \hat{O}_i$  is obtained using

$$P\hat{O}_{\text{eff}}P = P \sum_{i=1}^A \hat{O}_i P + P \sum_{i<j=1}^A \{e^{-S^{(2)}}(\hat{O}_i + \hat{O}_j)e^{S^{(2)}} - (\hat{O}_i + \hat{O}_j)\}P. \quad (18)$$

In general, to compute such a two-body correction to a one-body operator in our formalism is more involved than the evaluation of the effective interaction. This complexity arises because the transformation from relative plus c.m. coordinates to single-particle coordinates is needed in a sufficiently large two-nucleon space, typically comprising excitations up to several hundred  $\hbar\Omega$ . However, for a two-body operator depending on the relative position of two nucleons, the transformation is needed only in the model space typically comprising excitations of a few  $\hbar\Omega$ . It is for this simple reason

we choose to study initially the lowest-order renormalization for a two-body operator  $\hat{O} = \sum_{i<j=1}^A \hat{O}_{ij}$  depending on the relative position of two nucleons as, e.g., the point-nucleon rms radius operator. Here,

$$P\hat{O}_{\text{eff}}P = P \sum_{i<j=1}^A e^{-S^{(2)}} \hat{O}_{ij} e^{S^{(2)}} P. \quad (19)$$

We computed this term for the point-proton rms radius operator and discuss the results in the next section.

In any case, it should be realized that the operator renormalization is dependent on the model-space size and also on the HO frequency employed. As discussed in the next section, our ‘‘preferred’’ HO frequency occurs where the energy of the low-lying states in our largest spaces is approximately independent of the HO frequency. Sensibly, this preferred HO frequency is very close to the HO frequency obtained by phenomenological shell-model formulas. With that frequency we are able to obtain reasonably converged results even without operator renormalization.

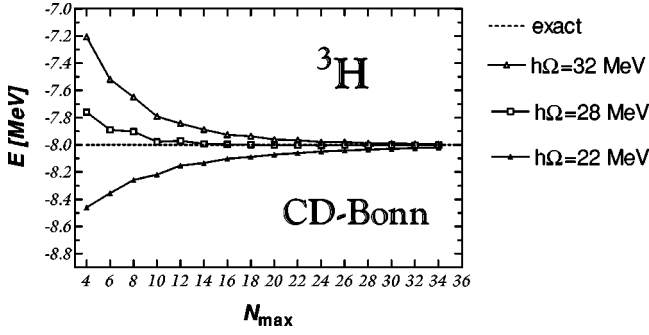


FIG. 1. The dependence of the  ${}^3\text{H}$  ground-state energy, in MeV, on the maximal number of HO excitations allowed in the model space in the range from  $N_{\text{max}}=4$  to  $N_{\text{max}}=34$ . The two-body effective interaction utilized was derived from the CD-Bonn  $NN$  potential. Results for  $\hbar\Omega=22$ , 28 and 32 MeV are presented. The dotted line represents the exact result of  $-8.00$  MeV from a 34-channel Faddeev-equation calculation [21].

#### D. Test of the method for the $A=3$ system

Before we proceed to apply the above approach to a complex system like  ${}^{12}\text{C}$ , we first test it for the simplest non-trivial case, the  $A=3$  system. In that case, we can study the detailed convergence properties of the method, as we are able to move up to very large model spaces. To perform the  $A=3$  calculations we employ the Jacobi-coordinate basis that is antisymmetrized according to the procedure introduced in Ref. [9].

The only parameters are the model space size, characterized by  $N_{\text{max}}$  and the HO frequency  $\Omega$ , appearing explicitly in the Hamiltonian (in terms that cancel algebraically, but are treated with separate methods) and in the basis. We investigate the dependence of our results on these two quantities as a measure of the validity of the two-body cluster approximation.

Let us consider  ${}^3\text{H}$  interacting by the CD-Bonn  $NN$  potential [21]. In Fig. 1 we show the  ${}^3\text{H}$  ground-state energy dependence on the model-space size in the range of  $N_{\text{max}}=4$  to 34. Different full lines connect results obtained with a specified HO frequency. The dotted line represents the CD-Bonn 34-channel Faddeev equation result of  $-8.00$  MeV [21]. It is apparent that our results converge to the Faddeev equation result as  $N_{\text{max}}$  increases. As stated earlier, the fundamental approximation used in our approach is to work only to the two-body-cluster level.

Our method is not a variational treatment. Therefore, we cannot expect a monotonic convergence from above. Three-body-cluster results for the ground-state energy could be either above or below the results at the two-body-cluster level. As seen from Fig. 1 our results converge with increasing  $N_{\text{max}}$  both from above or below, with some oscillations possible, depending on the HO frequency employed. Furthermore, we note that  $\hbar\Omega=28$  MeV provides results remarkably independent of  $N_{\text{max}}$  starting at rather low values of  $N_{\text{max}}\approx 10$ .

We note that even for the  $4\hbar\Omega$  model space, i.e.,  $N_{\text{max}}=4$ , the binding energy is within 10% of the exact result for a wide range of HO frequencies. For  $N_{\text{max}}\geq 6$  we see binding

errors less than 100 keV/nucleon and the errors decrease rapidly with  $N_{\text{max}}$  for these ‘‘sensible’’ choices of  $\Omega$ .

### III. RESULTS FOR ${}^{12}\text{C}$

The calculations for  ${}^{12}\text{C}$  were performed using the same approach that proved to be convergent for the  $A=3$  system. However, it is more efficient to perform the calculations in a single-particle HO basis, rather than in the Jacobi-coordinate HO basis used for  $A=3$ . We emphasize that our results are translationally invariant, because we employ a complete  $N\hbar\Omega$  model space and our effective interactions are translationally invariant. As mentioned above, we separate states with excited c.m. motion from those with the 0S c.m. motion by adding a term  $\Lambda(H_{\text{c.m.}} - \frac{3}{2}\hbar\Omega)$  to the Hamiltonian with  $\Lambda=10$ . However, our observable results are exactly corrected for the c.m. contributions and do not depend on  $\Lambda$ . In particular, for the form factors we use the correction discussed in Ref. [27]. Our calculations can, in principle, be redone in the relative-coordinate basis, producing the same results with a given effective Hamiltonian. Test calculations have been performed in  $A=3,4$  systems with both the Jacobi-coordinate HO basis and the single-particle HO basis with the same  $H_{\text{eff}}$  to confirm the above statement.

To study the influence of different  $NN$  potentials, we performed calculations using the CD-Bonn  $NN$  potential [21] and the Argonne V8'  $NN$  potential, defined in Ref. [4]. The CD-Bonn potential takes into account isospin-symmetry violations by both the strong and the electromagnetic interactions. The Argonne V8' potential is an isospin-invariant reduction of the Argonne V18  $NN$  potential. We, therefore, add the Coulomb interaction to the Argonne V8'. The calculations were performed in the proton-neutron formalism with the isospin breaking explicitly included, apart from the nucleon mass set equal to  $2m_p m_n / (m_p + m_n)$ . For the calculations with the CD-Bonn  $NN$  potential we compute three different effective interactions,  $V_{2\text{eff}}^{\text{np}}$ ,  $V_{2\text{eff}}^{\text{pp}}$ , and  $V_{2\text{eff}}^{\text{nn}}$ .

We employ the many-fermion dynamics shell-model code [28] to perform the Hamiltonian computation and diagonalization. Due to the increasing multiparticle model space size we are presently only able to use model spaces up through  $5\hbar\Omega$ .

As pointed out in the Sec. II D, there are only two parameters in our calculations, the model-space size ( $N_{\text{max}}$ ) and the HO frequency  $\Omega$  on which the effective interaction depends. As in the  $A=3$  test case, we investigate the dependence of the results on  $\Omega$  and the model-space size to the accessible limit. The  $N_{\text{max}}=0, 2$ , and 4 model spaces for the positive-parity states and the  $N_{\text{max}}=1, 3$ , and 5 model spaces for the negative-parity states are considered. Let us remark that the  $m$ -scheme dimensions grow from 51 in the  $0\hbar\Omega$  model space, 1320 in the  $1\hbar\Omega$  model space, 17725 in the  $2\hbar\Omega$  model space, 160084 in the  $3\hbar\Omega$  model space up to 1118926 in the  $4\hbar\Omega$  model space, and reach 6488004 in the  $5\hbar\Omega$  model space. For reference, the  $6\hbar\Omega$  model space dimension is 32598920.

In order to observe the dependence on the HO frequency  $\Omega$  we performed calculations using the above model spaces for a very wide range of  $\Omega$ . In Figs. 2 and 3, we present the

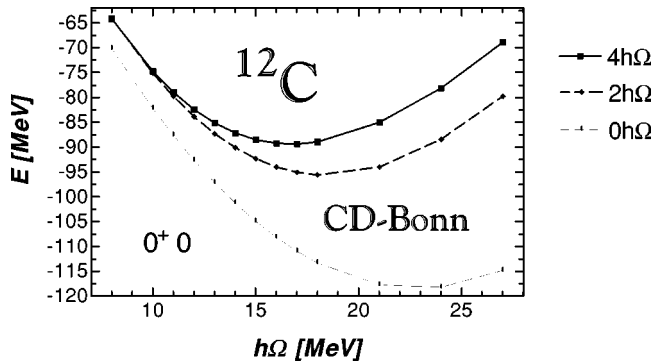


FIG. 2.  $^{12}\text{C}$  ground-state energy dependence on the HO frequency for the  $4\hbar\Omega$ ,  $2\hbar\Omega$ , and  $0\hbar\Omega$  model spaces calculated using the effective interaction derived from the CD-Bonn  $NN$  potential.

ground-state energy dependencies on the frequency for both the positive and the negative parity states, respectively, obtained using the CD-Bonn potential. The results for AV8 $'$  are very similar, although they exhibit a bit stronger dependence on  $\Omega$  most likely due to a stronger tensor force. In the subsequent calculations, we utilize  $\hbar\Omega = 15$  MeV which lies in the range where the largest model space results ( $N_{\text{max}} = 5$ ) are least sensitive to  $\hbar\Omega$ .

Let us remark that our preferred value of the HO frequency,  $\hbar\Omega = 15$  MeV, is close to the suggested value for  $A = 12$  given by the phenomenological relation [29] (in units of MeV):

$$\hbar\Omega = 45A^{-1/3} - 25A^{-2/3} \approx 14.9 \text{ MeV}. \quad (20)$$

In the next subsections we will investigate how several observables depend upon the HO frequency and model space size.

### A. Binding energy, excitation spectra, and EM transitions

From Figs. 2 and 3, we observe that, at fixed  $\hbar\Omega$ , the energy of the lowest eigenstate of each parity increases (i.e., becomes less negative) with increasing model space in most of the frequency range examined and the position of the

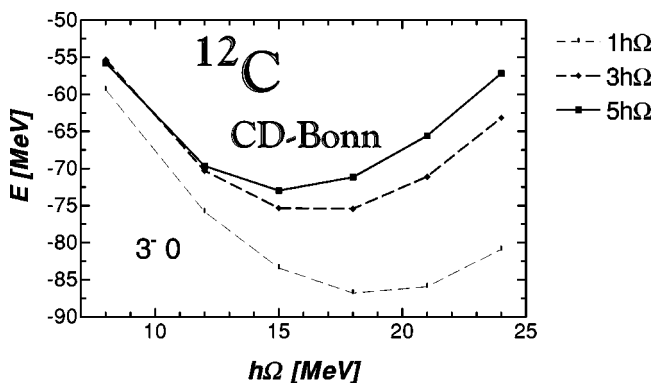


FIG. 3.  $^{12}\text{C}$   $3^-0$ -state energy dependence on the HO frequency for the  $5\hbar\Omega$ ,  $3\hbar\Omega$ , and  $1\hbar\Omega$  model spaces calculated using the effective interaction derived from the CD-Bonn  $NN$  potential.

minimum shifts to lower frequencies. Clearly, the difference between  $N_{\text{max}} = 2(3)$  and  $4(5)$  results is much smaller than between  $N_{\text{max}} = 0(1)$  and  $2(3)$ , results suggesting a convergence trend with increasing model space reminiscent of the trends shown in  $A = 3$  calculations (Fig. 1).

Our positive-parity state results, obtained with the preferred HO frequency  $\hbar\Omega = 15$  MeV, are presented in Table II and in Fig. 4, and the negative-parity state results, obtained using the same HO frequency, are given in Table III and Fig. 5. We discuss below results for the binding energies, point-proton rms radii,  $2_1^+$ -state quadrupole moments, and EM transitions.

From the observed trends in Table II and Fig. 2, we expect that our calculated binding energy of about 88 MeV for the preferred frequency in the  $4\hbar\Omega$  space will decrease with a further model-space enlargement. As discussed in Sec. II D, we estimate that our  $4\hbar\Omega$  result should be within 10% of the exact solution for the two-body  $NN$  potential utilized. Also, the  $4\hbar\Omega$  binding-energy values are probably more realistic than those obtained in the  $0\hbar\Omega$  or  $2\hbar\Omega$  space, as one expects roughly a 10–20% underbinding compared to the experimental value when a realistic two-body  $NN$  interaction is used alone. This is the trend found in lighter nuclei. In order to fit the experimental binding energy, it is likely that a true three-body  $NN$  interaction is necessary [4].

We note that we obtain a stronger binding for the CD-Bonn  $NN$  potential in agreement with observations for light nuclei, e.g., the  $^4\text{He}$  CD-Bonn binding energy is 26.3 MeV [10,32] while that of AV8 $'$  is 25.2 MeV [33]. On the other hand, based on these  $^4\text{He}$  results one would expect a larger difference in  $^{12}\text{C}$  between the binding energies from the two different interactions. Most likely, a different rate of convergence with increasing model space for the two utilized potentials may be responsible for smaller binding energy differences. Based on our  $A = 3, 4$  calculations, we expect a faster convergence for the CD-Bonn potential, which we attribute to its weaker tensor force.

In general, we obtain a reasonable agreement of the states dominated by  $0\hbar\Omega$  and  $1\hbar\Omega$  configurations with experimental levels. We also observe a general trend of improvement with increasing model space size, in particular, for the  $T = 1$  states. While the energy of the lowest eigenstate of each parity increases with increasing model space, the relative level spacings are less dependent on the model space size.

As a gauge of trends with increasing model space size, consider the rms changes in excitation energies of the first seven excited states of each parity in the CD-Bonn case. For positive parity states, the rms changes are 1.31 (0.22) MeV in going from 0 to 2 (2 to 4) $\hbar\Omega$ . For negative parity states, the rms changes are 0.87 (0.20) MeV in going from 1 to 3 (3 to 5) $\hbar\Omega$ . The difference between the  $N_{\text{max}} = 2(3)$  and  $4(5)$  results is significantly smaller than that between the  $N_{\text{max}} = 0(1)$  and  $2(3)$  results which is similar to the convergence trends we saw in lighter systems [6,9,10]. Our computed  $T = 0$   $0^+, 2^+, 4^+$  band has a reasonable splitting. We obtain a reasonable set of excitation energies for the  $T = 1$  states relative to the lowest  $T = 0$  state of each parity. In addition, our

TABLE II. Experimental and calculated binding energies, ground-state point-proton rms radii, the  $2_1^+$ -state quadrupole moments, as well as  $E2$  transitions, in  $e^2 \text{ fm}^4$ , and  $M1$  transitions, in  $\mu_N^2$ , of  $^{12}\text{C}$ . Results obtained in different model spaces, i.e.,  $N_{\text{max}}=4,2,0$ , and using effective interactions derived from the CD-Bonn and the Argonne V8'  $NN$  potentials are compared. A HO frequency of  $\hbar\Omega=15$  MeV was employed. The experimental values are from Refs. [30,31].

Model space	$^{12}\text{C}$			CD-Bonn			AV8'		
	$4\hbar\Omega$	$2\hbar\Omega$	$0\hbar\Omega$	$4\hbar\Omega$	$2\hbar\Omega$	$0\hbar\Omega$	$4\hbar\Omega$	$2\hbar\Omega$	$0\hbar\Omega$
$ E_{\text{g.s.}} $ (MeV)	92.162	88.518	92.353	104.947	87.675	92.195	104.753		
$r_p$ (fm)	2.35(2)	2.199	2.228	2.376	2.202	2.228	2.376		
$Q_{2^+}$ ( $e \text{ fm}^2$ )	+6(3)	4.533	4.430	4.253	4.536	4.427	4.250		
$E_x(0^+0)$ (MeV)	0.0	0.0	0.0	0.0	0.0	0.0	0.0		
$E_x(2^+0)$ (MeV)	4.439	3.697	3.837	3.734	3.584	3.766	3.699		
$E_x(1^+0)$ (MeV)	12.710	14.141	14.525	13.866	14.044	14.549	13.935		
$E_x(4^+0)$ (MeV)	14.083	13.355	13.636	12.406	12.848	13.255	12.192		
$E_x(1^+1)$ (MeV)	15.110	16.165	16.291	15.290	16.295	16.515	15.488		
$E_x(2^+1)$ (MeV)	16.106	17.717	17.945	15.970	17.945	17.823	15.920		
$E_x(0^+1)$ (MeV)	17.760	16.618	16.493	14.698	16.205	16.208	14.574		
$B(E2;2^+0 \rightarrow 0^+0)$	7.59(42)	4.625	4.412	4.092	4.612	4.397	4.091		
$B(M1;1^+0 \rightarrow 0^+0)$	0.0145(21)	0.0042	0.0032	0.0013	0.0026	0.0019	0.0008		
$B(M1;1^+0 \rightarrow 2^+0)$	0.0081(14)	0.0017	0.0013	0.0008	0.0013	0.0012	0.0008		
$B(M1;1^+1 \rightarrow 0^+0)$	0.951(20)	0.355	0.280	0.158	0.316	0.252	0.147		
$B(M1;1^+1 \rightarrow 2^+0)$	0.068(9)	0.0002	0.0028	0.0115	0.0023	0.0078	0.0167		
$B(E2;2^+1 \rightarrow 0^+0)$	0.65(13)	0.283	0.015	0.0018	0.104	0.000	0.002		

lowest  $0^+$   $T=2$  state lies between 27 and 29 MeV, depending on the  $NN$  potential and the model space, in good agreement with the experimental  $0^+2$  state at 27.595 MeV.

We note that the favorable comparison with available data is a consequence of the underlying  $NN$  interaction rather than a phenomenological fit.

Our ground-state wave function in the  $4\hbar\Omega$  calculation consists of 61% of  $0\hbar\Omega$  configurations. The occupancy of the  $0p3/2$  level is about 5.74 nucleons, while the occupancy of the  $0p1/2$  level is about 1.90 nucleons.

For the  $T=0$  negative-parity states we obtain the correct sequence of the excited states compared to the experiment.

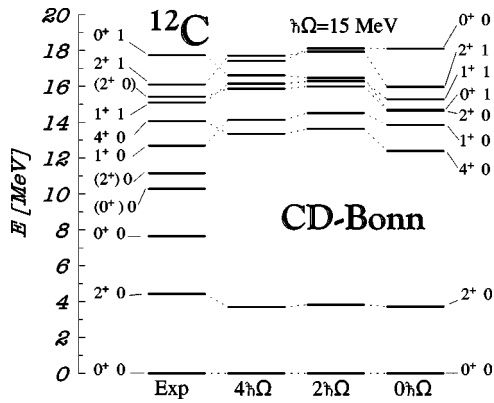


FIG. 4. Experimental and theoretical positive-parity excitation spectra of  $^{12}\text{C}$ . Results obtained in  $4\hbar\Omega$ ,  $2\hbar\Omega$ , and  $0\hbar\Omega$  model spaces are compared. The effective interaction was derived from the CD-Bonn  $NN$  potential in a HO basis with  $\hbar\Omega=15$  MeV. The experimental values are from Ref. [30].

The ordering of the  $T=1$  states improves with the model-space increase. In the calculation, we see a  $0^-0$  and a second  $3^-0$  state below 8 MeV excitation relative to the lowest  $3^-0$  state. Such states are not presently known experimentally.

In Fig. 6 we present the evolution of the lowest positive and negative parity states of a given isospin with the model-space change computed using the same  $\hbar\Omega=15$  MeV. While the position of the  $1^+1$  is fairly stable, it is clear that the excitation energies of the negative-parity states relative to the positive-parity states decrease rapidly with the model-space size enlargement. Still, even in our largest spaces the  $3^-0$  state is more than 5 MeV too high compared to the experimental excitation energy.

The spectra obtained in the  $4\hbar\Omega$  space using the CD-Bonn and Argonne V8'  $NN$  potentials are compared in Fig. 7. There is remarkably little difference between the results from the two  $NN$  interactions, although the overall agreement with experiment is slightly better for the CD-Bonn  $NN$  potential, in particular for the  $T=1$  states. This also is true for the negative-parity states. It should be noted, however, that the position and ordering of the  $T=1$  states improves with the enlargement of the model space for both potentials.

In order to achieve a more converged excitation spectra a still larger model space is needed, especially for states with significant cluster structure. The two- and higher- $\hbar\Omega$  dominated states, such as the 7.65 MeV  $0^+0$  state that is known to be a three- $\alpha$  cluster resonance [34], are not seen in the low-lying part of our calculated spectra. In general, the convergence rate of the  $2\hbar\Omega$  dominated states is quite different than that of the ground state, as we observed in  $^4\text{He}$  calculations performed in the present formalism [9,10]. Also, a

TABLE III. Experimental and calculated negative-parity state energies, the  $3^-0$ -state point-proton rms radii, and quadrupole moments are shown. Results obtained in different model spaces, i.e.,  $N_{\max}=5,3,1$ , and using effective interactions derived from the CD-Bonn and the Argonne V8'  $NN$  potentials are compared. The calculated excitation energy of the  $3^-0$  state is obtained by comparing its energy in the  $N\hbar\Omega$  space with the ground state in the  $(N-1)\hbar\Omega$  space. A HO frequency of  $\hbar\Omega=15$  MeV was employed. The experimental values are taken from Ref. [30].

Model space	$^{12}\text{C}$		CD-Bonn			AV8'	
	$5\hbar\Omega$	$3\hbar\Omega$	$1\hbar\Omega$	$5\hbar\Omega$	$3\hbar\Omega$	$1\hbar\Omega$	
$ E(3^-0) $ (MeV)	82.521	72.952	75.331	83.390	72.300	75.360	83.459
$r_p$ (fm)		2.309	2.316	2.425	2.310	2.315	2.425
$Q_{3^-}$ ( $e\text{ fm}^2$ )		-7.942	-7.596	-6.936	-7.920	-7.575	-6.933
$E(3^-0)-E_{\text{gs}}$ (MeV)	9.641	15.566	17.022	21.557	15.375	16.835	21.294
$E_x(3^-0)$ (MeV)	0.0	0.0	0.0	0.0	0.0	0.0	0.0
$E_x(1^-0)$ (MeV)	1.203	2.093	2.256	1.561	2.112	2.274	1.552
$E_x(2^-0)$ (MeV)	2.187	3.722	4.051	3.582	3.722	4.057	3.567
$E_x(4^-0)$ (MeV)	3.711	4.866	5.084	4.768	4.741	4.993	4.710
$E_x(0^-0)$ (MeV)		7.148	7.062	5.712	7.148	7.156	5.777
$E_x(2^-1)$ (MeV)	6.929	7.671	7.783	7.340	7.949	8.237	7.574
$E_x(3^-0)$ (MeV)		7.877	8.151	6.886	7.651	7.983	6.745
$E_x(1^-1)$ (MeV)	7.589	8.048	7.951	7.042	8.117	8.096	7.184

preferred HO frequency for the convergence of the ground state will differ from the preferred frequency for the  $2\hbar\Omega$  states.

We investigated the position of the lowest  $2\hbar\Omega$  dominated states and the giant-quadrupole resonance (GQR)  $E2$  distribution. Our lowest  $2\hbar\Omega$   $0^+$  state lies at about 40 MeV excitation energy and the GQR  $E2$  strength is distributed between 43 to 50 MeV in the  $2\hbar\Omega$  calculation. In the  $4\hbar\Omega$  model space the excitation energy of the lowest  $2\hbar\Omega$   $0^+$  state drops by 5 MeV to about 35 MeV and, similarly, the GQR strength is lowered to 37–47 MeV. We present our calculated  $E2$  strength obtained in the  $4\hbar\Omega$  model space using the CD-Bonn potential and  $\hbar\Omega=14$  MeV in Fig. 8. We note that the experimental GQR strength is observed in the range 18–28 MeV [35]. Our trends indicate the probable need for several more major shells to hope to achieve a favorable description of the  $E2$  strength distribution.

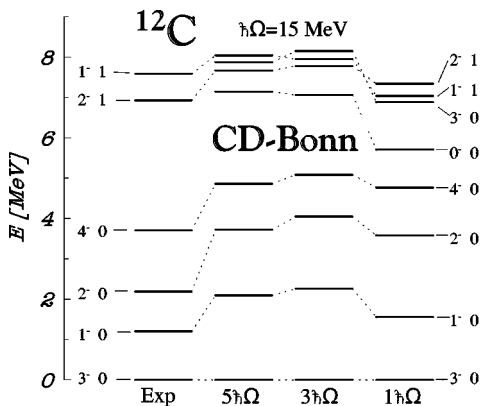


FIG. 5. Experimental and theoretical negative-parity spectra of  $^{12}\text{C}$ . Results obtained in  $5\hbar\Omega$ ,  $3\hbar\Omega$ , and  $1\hbar\Omega$  model spaces are compared. Other factors are the same as in Fig. 4.

Our radius and  $E2$  results, based on the bare radius operator and bare nucleon charges, are smaller than the experimental values. The underestimation of the rms radius, the quadrupole moment and the  $E2$  transitions is linked with the overestimation of the position of the GQR strength and suggests that even in the  $N_{\max}=4$  space we still miss significant  $\alpha$  clustering effects. We also observe a strong model space dependence of the  $M1$  transitions,  $1^+1 \rightarrow 0^+0$ . Clearly, there is still a need for effective operators, which are calculable within our theoretical framework, as discussed in Sec. II C.

We computed the two-body-cluster term (19) for the point-proton rms radius operator and found that the renormalization leads to an increase of the radius and that the size of this increase drops as the model space size increases. In particular, the  $r_p$  results presented in Table II that were ob-

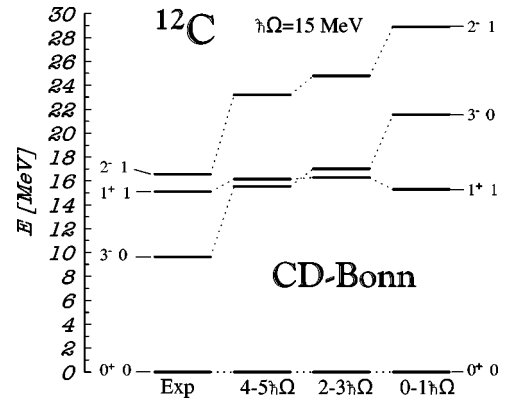


FIG. 6. Experimental and theoretical excitation spectra of  $^{12}\text{C}$ . Results for the lowest states of given isospin and of both positive and negative parity obtained in the model spaces from  $0\hbar\Omega$  to  $5\hbar\Omega$  are shown. All other factors are the same as in Fig. 4.

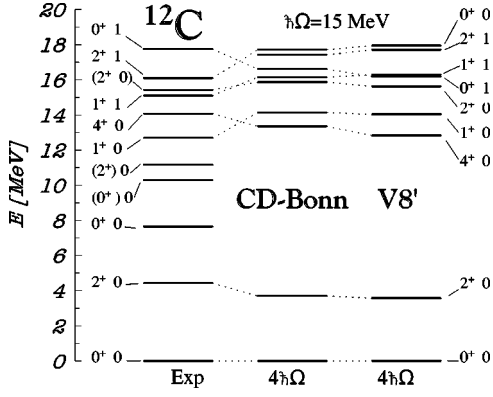


FIG. 7. Experimental and calculated excitation spectra of  $^{12}\text{C}$ . Results obtained using the effective interactions derived from the CD-Bonn  $NN$  potential and the Argonne V8'  $NN$  potential are compared. A  $4\hbar\Omega$  model space and a HO frequency of  $\hbar\Omega = 15$  MeV were used. The experimental values are taken from Ref. [30].

tained without renormalization should be increased due to the renormalization by about 0.06, 0.02, and 0.01 fm for the  $N_{\text{max}}=0, 2, \text{ and } 4$  model spaces, respectively. This does not imply that the renormalization of other operators, e.g., the  $E2$  operator, cannot be substantially higher. Also, we note that the renormalization is HO frequency dependent. Similarly, as observed in our  $^3\text{H}$  calculations, e.g., compare Figs. 1 and 4 in Ref. [10], we anticipate that, in contrast with the eigenenergies, the other observables will change more significantly as we move to larger model spaces and/or larger clusters in the effective Hamiltonian and other operators.

A brief examination of the radius and  $B(E2)$  to the ground state proves instructive. If one takes the  $4\hbar\Omega$  results for CD-Bonn from Table I and scales the calculated  $B(E2)$  ( $4.625e^2 \text{ fm}^4$ ) by the fourth power of the ratio of the experimental point-proton radius to the calculated point-proton radius ( $2.35/2.199$ ), we diminish the discrepancy between theory and experiment by more than 50%. This indicates that when we find the source of improvement in the point-proton radius, it is also likely to improve the value for the  $B(E2)$ .

The sensitivity of observables to the HO frequency can be judged from Table IV. There, we present selected observables obtained in calculations with the CD-Bonn  $NN$  poten-

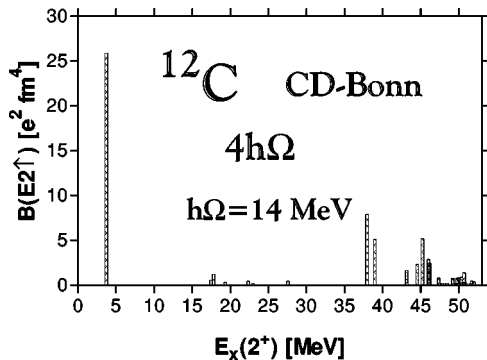


FIG. 8. Calculated  $E2$  strength obtained in the  $4\hbar\Omega$  model space using the CD-Bonn potential and  $\hbar\Omega = 14$  MeV.

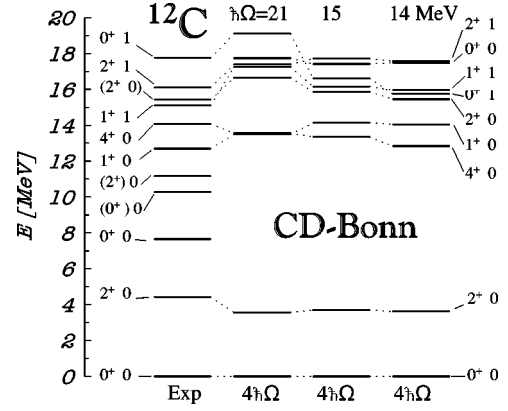


FIG. 9. Experimental and calculated excitation spectra of  $^{12}\text{C}$ . Results obtained using the HO frequencies  $\hbar\Omega = 14, 15, 21$  MeV are compared. The effective interaction was derived from the CD-Bonn  $NN$  potential. A model space of  $4\hbar\Omega$  above the unperturbed ground state was used. The experimental values are taken from Ref. [30].

tial for three different HO frequencies,  $\hbar\Omega = 14, 15, \text{ and } 21$  MeV and for the  $N_{\text{max}}=0, 2, \text{ and } 4$  model spaces. We observe that, indeed, the dependence of the results on  $\Omega$  decreases as the model space is enlarged. This is true, in particular, for the binding energies, radii, and the quadrupole moments. On the other hand, it is obvious that the  $4\hbar\Omega$  model space is not sufficient to obtain fully convergent results. The corresponding excitation spectra dependence on the HO frequency is presented in Fig. 9, where we show results obtained in the  $4\hbar\Omega$  model space for the above three values of  $\Omega$ . It appears that the overall agreement with experiment is the most favorable for our preferred HO frequency  $\hbar\Omega = 15$  MeV.

From Table IV, we also note a strong dependence of the  $M1$  transitions, e.g.,  $1^+1 \rightarrow 0^+0$ , on  $\Omega$ . This dependence is stronger than the dependence on the particular change in model-space size, displayed in Table II. Overall, the  $M1$  transitions are closer to experiment for larger  $\Omega$ , while just the opposite trend is seen for the  $E2$  transitions. This trend in results correlates with the change of relative occupation of the  $0p3/2$  and the  $0p1/2$  levels. With larger  $\Omega$  more nucleons tend to occupy the  $0p3/2$  level and the rate of the  $M1$  transition increases.

Let us further comment on the  $E2$  transition  $2^+1 \rightarrow 0^+0$ . In Table II we present the transitions from the lowest calculated  $2^+1$  state. There is a level crossing, however, so that in the  $2\hbar\Omega$  and  $0\hbar\Omega$  model spaces, the calculated  $2^+1$  state with a strong  $E2$  transition to the ground state is the second  $2^+1$  state.

## B. Elastic charge form factors

Parity-violating elastic electron scattering experiments on even-even,  $N=Z$  nuclei, like  $^{12}\text{C}$ , provide a test of the neutral current sector of the standard model. The observable of interest is the parity-violating asymmetry

$$A = \frac{d\sigma_+ - d\sigma_-}{d\sigma_+ + d\sigma_-} = -\frac{G_\mu q^2}{4\pi\alpha\sqrt{2}} \left( \frac{\tilde{F}_C(q)}{F_C(q)} - \frac{F_C^{(s)}(q)}{F_C(q)} + \dots \right), \quad (21)$$

TABLE IV. Calculated ground-state point-proton rms radii, the  $2_1^+$ -state quadrupole moments, as well as  $E2$  transitions, in  $e^2 \text{ fm}^4$ , and  $M1$  transitions, in  $\mu_N^2$ , of  $^{12}\text{C}$ . Results obtained in different model spaces, i.e.,  $4\hbar\Omega$ ,  $2\hbar\Omega$ , and  $0\hbar\Omega$ , using different HO frequencies, i.e.,  $\hbar\Omega = 21, 15$ , and  $14 \text{ MeV}$ , are compared. The effective interactions used were derived from the CD-Bonn  $NN$  potential. The corresponding experimental values are presented in Table II.

Model space $\hbar\Omega$ (MeV)	$4\hbar\Omega$			$2\hbar\Omega$			$0\hbar\Omega$		
	21	15	14	21	15	14	21	15	14
$ E_{\text{g.s.}} $ (MeV)	85.054	88.518	87.145	94.006	92.353	90.110	117.744	104.947	101.275
$r_p$ (fm)	1.978	2.199	2.260	1.932	2.228	2.301	2.008	2.376	2.459
$Q_{2^+}$ ( $e \text{ fm}^2$ )	3.587	4.533	4.792	3.318	4.430	4.718	2.970	4.253	4.568
$B(E2; 2^+0 \rightarrow 0^+0)$	2.917	4.625	5.178	2.488	4.412	5.016	1.994	4.092	4.722
$B(M1; 1^+1 \rightarrow 0^+0)$	0.683	0.355	0.305	0.657	0.280	0.237	0.357	0.158	0.137

where  $+$  ( $-$ ) refers to electrons polarized parallel (antiparallel) to their momenta. In Eq. (21),  $F_C(q)$  denotes the EM charge form factor, while the weak neutral form factor is split into two components, the strangeness charge form factor  $F_C^{(s)}(q)$  and the form factor  $\tilde{F}_C(q)$ , given by combination of the EM isoscalar and isovector form factors, as discussed in Refs. [14,36]. For an isospin invariant system, the ratio  $\tilde{F}_C(q)/F_C(q)$  is equal to  $-4 \sin^2 \theta_w$ . Isospin-symmetry violation leads to a correction  $\Gamma$  to this value, defined by the relation

$$\frac{\tilde{F}_C(q)}{F_C(q)} = -4 \sin^2 \theta_w (1 + \Gamma). \quad (22)$$

The evaluation of form factors with unrenormalized operators is a sensitive test of the  $P$ -space wave functions obtained in our calculations. Using the formalism of Ref. [17], we calculated the elastic charge EM and weak neutral form factors in the impulse approximation. The one-body contribution to the charge operator is given by Eq. (15) in Ref. [17], e.g.,

$$\hat{M}_{00}^{(a)}(q)^{[11]} = \frac{1}{2\sqrt{\pi}} \sum_{k=1}^A \hat{O}_k^{(a)} \left\{ \frac{G_E^{(a)}(\tau)}{\sqrt{1+\tau}} j_0(qr_k) + [G_E^{(a)}(\tau) - 2G_M^{(a)}(\tau)] 2\tau \frac{j_1(qr_k)}{qr_k} \boldsymbol{\sigma}_k \cdot \mathbf{L}_k \right\}, \quad (23)$$

where  $\tau = q^2/4m_N^2$ ,  $\mathbf{L}_k$  is the  $k$ th nucleon orbital momentum and  $G_E^{(a)}(\tau)$  and  $G_M^{(a)}(\tau)$  are the one-body electric and magnetic form factors, respectively. The superscript ( $a$ ) refers to ( $p$ ) and ( $n$ ) for proton and neutron EM form factors, respectively, or to ( $s$ ) for the strangeness form factor. The operator  $\hat{O}^{(a)}$  is equal to  $(\frac{1}{2} + t_z)$  [ $(\frac{1}{2} - t_z)$ ] for  $a \equiv p$  ( $a \equiv n$ ) and it is equal to 1 for  $a \equiv s$ . The one-body form factors  $\tilde{G}_{E,M}^{(p,n)}(q)$ , needed for evaluating  $\tilde{F}_C(q)$ , are obtained as combinations of the EM one-body form factors [14,36]. The charge form factors are given as  $F_C^{(a)}(q) = 2\sqrt{\pi} \langle 0^+ | \hat{M}_{00}^{(a)}(q)^{[11]} | 0^+ \rangle$ . We use the parametrization of the one-body form factors, as discussed in Ref. [17].

We note that the one-body strangeness form factors depend on the strangeness radius  $\rho_s$  and on the strangeness magnetic moment  $\mu_s$ . Limits on these parameters are to be determined in experiments at the Thomas Jefferson Accelerator Facility. The first strangeness magnetic-moment measurements were reported recently [37]. In our calculations we investigate the sensitivity of the  $^{12}\text{C}$  form factor ratios to these parameters.

The elastic EM charge form factors of  $^{12}\text{C}$  are presented in Figs. 10 and 11. Note that the squared longitudinal form factor  $F_L^2 = (F_C/Z)^2$  is displayed in Fig. 10, where we compare our calculated form factor, obtained in the impulse approximation, with the experimental data. The wave function used was obtained in the  $4\hbar\Omega$  calculation with the effective interaction derived from the CD-Bonn  $NN$  potential and with  $\hbar\Omega = 14 \text{ MeV}$ . Note that, as seen in Table IV, the  $4\hbar\Omega$  result for the  $^{12}\text{C}$  charge radius is closer to the experimental result of  $2.309 \text{ fm}$  with  $\hbar\Omega = 14 \text{ MeV}$  ( $r_p = 2.260 \text{ fm}$ ) than with  $\hbar\Omega = 15 \text{ MeV}$  ( $r_p = 2.199 \text{ fm}$ ). We miss the experimental minimum slightly and underestimate the second maximum. This may be due in part to the omission of the MEC, but, more likely, are due to an incomplete conver-

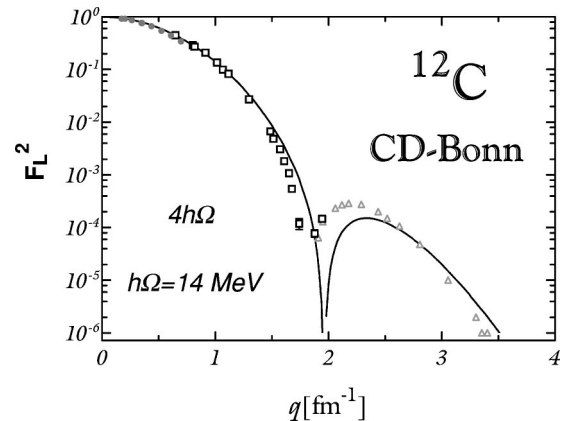


FIG. 10. The experimental and calculated values of the elastic EM charge form factor of  $^{12}\text{C}$  are presented. The calculation, done in the impulse approximation, was performed using the two-body effective interaction derived from the CD-Bonn  $NN$  potential in a model space of  $4\hbar\Omega$  excitations above the unperturbed ground state. A HO frequency  $\hbar\Omega = 14 \text{ MeV}$  was used. The experimental values are taken from Ref. [38].

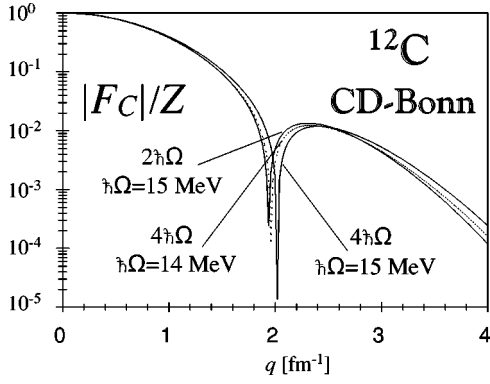


FIG. 11. The elastic EM charge form factor of  $^{12}\text{C}$  calculated in the impulse approximation. The calculations were performed using the two-body effective interaction derived from the CD-Bonn  $NN$  potential. Results obtained in model spaces of  $2\hbar\Omega$  and  $4\hbar\Omega$  excitations above the unperturbed ground state and with different HO frequencies of  $\hbar\Omega = 14$  and  $15$  MeV are compared.

gence of our wave function and the need for three-body forces. A separate issue to be addressed in the future, is the renormalization of the operator (23) due to the space truncation, as discussed in Sec. II C.

The sensitivity of the form factor on the model-space size and on the HO frequency can be judged from Fig. 11. Results obtained in the  $2\hbar\Omega$  and  $4\hbar\Omega$  model spaces are compared. In addition, calculations using our preferred HO frequency  $\hbar\Omega = 15$  MeV and the frequency  $\hbar\Omega = 14$  MeV employed in Fig. 10 are shown. The curves differ for  $q > 1.4 \text{ fm}^{-1}$ , as a result of incomplete convergence of the wave functions since converged results should be independent of  $\hbar\Omega$ . The trend of moving the dip to smaller  $q$  with decreasing  $\hbar\Omega$  and fixed  $N_{\text{max}}$  may be understood easily in terms of the charge radius trend with decreasing  $\hbar\Omega$  mentioned above. A similar correspondence of trends with changing  $N_{\text{max}}$  is observed in Fig. 11.

The calculated isospin-breaking correction  $\Gamma$  is shown in Fig. 12. Our result, obtained again in the impulse approximation using the  $4\hbar\Omega$  model space with the effective interaction derived from the CD-Bonn  $NN$  potential and  $\hbar\Omega = 15$  MeV, compares very well up to  $q \approx 3 \text{ fm}^{-1}$  with that calculated by Ormand [36] using the Hartree-Fock approach.

In Fig. 13, we present the elastic strangeness charge form factor, obtained in the impulse approximation using the  $4\hbar\Omega$  model space and  $\hbar\Omega = 15$  MeV. To study the sensitivity to the  $NN$  potential, we performed the calculations with the CD-Bonn  $NN$  potential and the Argonne V8'  $NN$  potential. We observe only a very weak dependence on the  $NN$  potential, unlike for light nuclei with  $A = 3, 4$  [10]. Such a weak dependence is obtained not only for the strangeness form factor, but also for the EM form factor of  $^{12}\text{C}$ .

In Figs. 14 and 15 we present the ratio of the  $^{12}\text{C}$  strangeness and EM charge form factors calculated in the impulse approximation using the CD-Bonn  $NN$  potential. As discussed in the beginning of this subsection, the ratio of the elastic charge form factors is particularly interesting, as it can be experimentally obtained from the measurement of the parity-violating left-right asymmetry for the scattering of po-

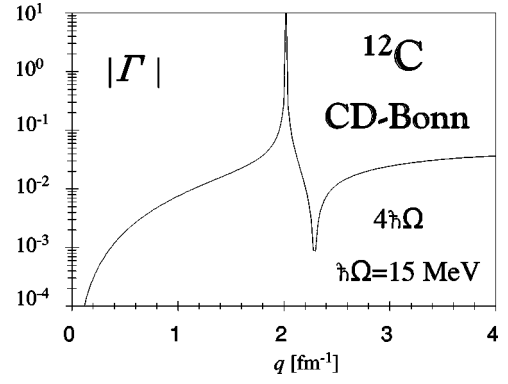


FIG. 12. The isospin breaking correction  $\Gamma$  depending on the ratio of elastic weak and EM charge form factors of  $^{12}\text{C}$  is presented. The calculations done in the impulse approximation were performed using the two-body effective interaction derived from the CD-Bonn  $NN$  potential in a model space of  $4\hbar\Omega$  excitations above the unperturbed ground state. A HO frequency  $\hbar\Omega = 15$  MeV was used.

larized electrons from a  $^{12}\text{C}$  target. The sensitivity to  $\mu_s$  is the strongest in the vicinity of the second maximum. However, it is weaker in  $^{12}\text{C}$  than in  $^4\text{He}$ , as seen by comparing the results presented in Ref. [17]. On the other hand, the sensitivity to  $\rho_s$  is substantial also in  $^{12}\text{C}$ , in particular, beyond the minimum.

#### IV. CONCLUSIONS

We introduced the *ab initio* no-core shell model and performed large-basis calculations for  $^{12}\text{C}$  in the model spaces up to  $4\hbar\Omega$  for the positive-parity states and up to  $5\hbar\Omega$  for the negative-parity states. The two-body effective interactions for each model space were derived microscopically from modern  $NN$  potentials using a unitary transformation of the Hamiltonian and the model-space decoupling condition,

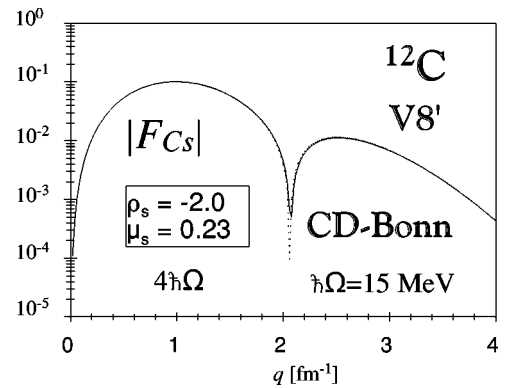


FIG. 13. The elastic strangeness charge form factor of  $^{12}\text{C}$  calculated in the impulse approximation. The calculations were performed in a model space of  $4\hbar\Omega$  excitations above the unperturbed ground state and with a HO frequency of  $\hbar\Omega = 15$  MeV. Results obtained using the two-body effective interaction derived from the CD-Bonn (full line) and Argonne V8' (dotted line)  $NN$  potentials are compared. The values of the strangeness radius  $\rho_s = -2.0$  and of the strangeness magnetic moment  $\mu_s = 0.23$  were employed.

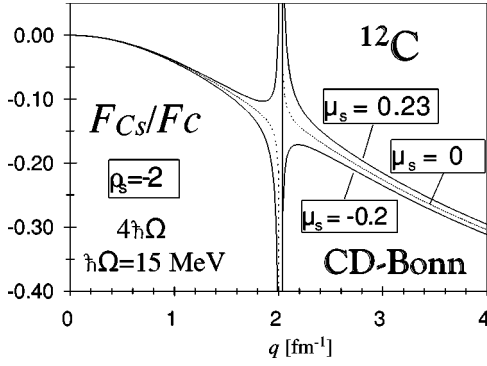


FIG. 14. The ratio of elastic strangeness and EM charge form factors of  $^{12}\text{C}$  calculated in the impulse approximation. The value of the strangeness radius  $\rho_s = -2.0$  was employed. The different curves correspond to different strangeness magnetic moments, e.g.,  $\mu_s = -0.2, 0.0,$  and  $0.23$ . The calculations were performed using the two-body effective interaction derived from the CD-Bonn  $NN$  potential in the model space of  $4\hbar\Omega$  excitations above the unperturbed ground state. A HO frequency  $\hbar\Omega = 15$  MeV was used.

which is fulfilled at the two-body cluster level. This method, which we also applied in our earlier studies, converges to the exact solution for increasing size of the model space, as we demonstrated for the  $A = 3$  and  $4$  systems.

We note that we performed no-core shell-model calculations for the  $0p$ -shell nuclei in the past [6–8] using a similar approach as that discussed here. In those calculations, however, an additional adjustable parameter was present, i.e., the “starting energy” of the two-body  $G$  matrix. Thus, in general, convergence to the exact solutions would have been difficult to demonstrate.

In the present application, a two-body cluster approximation results in a dependence on the size of the model-space and on the HO frequency. We selected a preferred HO frequency by examining where the ground-state energy is least dependent on the frequency in our largest model spaces. The resulting value  $\hbar\Omega \approx 15$  MeV is in accord with values sug-

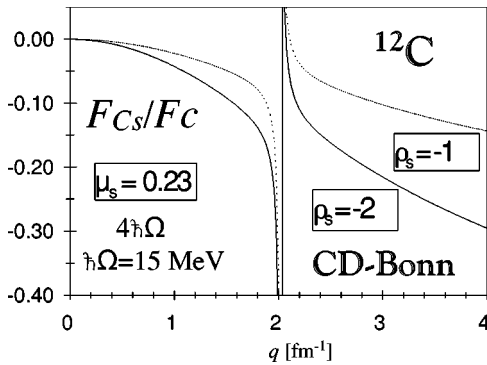


FIG. 15. The ratio of elastic strangeness and EM charge form factors of  $^{12}\text{C}$  calculated in the impulse approximation. The value of the strangeness magnetic moment  $\mu_s = 0.23$  was employed. The different curves correspond to different strangeness radii, e.g.,  $\rho_s = -1.0$  and  $-2.0$ . The calculations were performed using the two-body effective interaction derived from the CD-Bonn  $NN$  potential in the model space of  $4\hbar\Omega$  excitations above the unperturbed ground state. A HO frequency  $\hbar\Omega = 15$  MeV was used.

gested by phenomenological shell-model formulas.

Using results for  $A = 3$  and  $4$ , we analyzed the deviations in binding energy per nucleon at the preferred value of  $\hbar\Omega$  and found a suppression of the changes that arise at the three-body or four-body cluster level. Overall, we estimate that the uncertainty in our  $4\hbar\Omega$  binding energy for  $^{12}\text{C}$  due to truncation at the two-body cluster level is less than 10%.

The  $^{12}\text{C}$  results that we obtained are not fully convergent with respect to increasing model-space size. In spite of this, we expect that we have obtained a reasonable approximation to the exact results for the  $0\hbar\Omega$ - and  $1\hbar\Omega$ -dominated states. In fact, we also obtained a reasonable agreement of the states dominated by  $0\hbar\Omega$  and  $1\hbar\Omega$  configurations with experimental levels. We note that the favorable comparison with available data is a consequence of the underlying  $NN$  interaction rather than a phenomenological fit. The positive-parity low-lying states of  $^{12}\text{C}$  that are dominated by the higher-than- $0\hbar\Omega$  components were not observed among our low-lying calculated states. Convergence of such states in the HO basis expansion is much slower with increasing model-space size. Our computed negative-parity states were shifted to higher energies by only a few MeV compared with experiment and were generally in the correct order.

Apart from the binding and excitation energies, we also studied the EM properties and the point-proton rms radii. In addition, we computed elastic charge form factors in the impulse approximation that are relevant to parity-violating electron scattering studies. We presented results for the EM and weak neutral form factors of  $^{12}\text{C}$ . We observed that the dependence of the form factor ratio  $F_C^{(s)}/F_C$  on the strangeness magnetic moment is weaker for  $^{12}\text{C}$  than for  $^4\text{He}$ . On the other hand, the dependence on the strangeness radius remains strong also for  $^{12}\text{C}$ .

We demonstrated that the multiconfiguration no-core shell-model approach combined with the use of microscopic effective interactions is well suited for the description of electron scattering or other electroweak processes from complex light nuclei, like  $^{12}\text{C}$ . In particular, we treat the c.m. motion properly, so that our calculated form factors do not depend on the c.m. motion. In addition, the utilization of large model spaces improves the justification for the employment of unrenormalized transition operators. In the present study we performed our calculations in the impulse approximation. The MEC contributions can also be included in our approach and will be the subject of a subsequent study.

Our wave functions along with the one-body and two-body densities can also be used for evaluating the neutrino and muon reactions with  $^{12}\text{C}$ . Such studies will be a subject of future investigations. It is challenging, but not impossible, to extend the present calculations to even larger model spaces, e.g.,  $6\hbar\Omega$ . This would be important, as we noted that our results were not fully converged, even in the case of the  $0\hbar\Omega$ -dominated states. In addition, the positive-parity higher- $\hbar\Omega$ -dominated states were not observed in the low-lying part of our calculated spectra. A further increase of the model-space size should result in the lowering of their energy. This investigation is in progress.

## ACKNOWLEDGMENTS

This work was supported in part by NSF Grant No. PHY96-05192 and in part by U.S. DOE Grant No. DE-FG-02-87ER-40371, Division of High Energy and Nuclear Phys-

ics. J.P.V. acknowledges valuable technical assistance from J.J. Coyle and D.R. Fils. We thank the DOE's Institute for Nuclear Theory at the University of Washington for its hospitality and the Department of Energy for partial support during the completion of this work.

- 
- [1] L. D. Faddeev, Zh. Éksp. Teor. Fiz. **39**, 1459 (1960) [Sov. Phys. JETP **12**, 1014 (1961)]; J. L. Friar, G. L. Payne, V. G. J. Stoks, and J. J. de Swart, Phys. Lett. B **311**, 4 (1993); A. Nogga, D. Hüber, H. Kamada, and W. Glöckle, *ibid.* **409**, 19 (1997).
- [2] O. A. Yakubovsky, Yad. Fiz. **5**, 1312 (1966) [Sov. J. Nucl. Phys. **5**, 937 (1967)]; W. Glöckle and H. Kamada, Phys. Rev. Lett. **71**, 971 (1993).
- [3] M. Viviani, A. Kievsky, and S. Rosati, Few-Body Syst. **18**, 25 (1995); N. Barnea, W. Leidemann, and G. Orlandini, Nucl. Phys. **A650**, 427 (1999).
- [4] B. S. Pudliner, V. R. Pandharipande, J. Carlson, S. C. Pieper, and R. B. Wiringa, Phys. Rev. C **56**, 1720 (1997); R. B. Wiringa, Nucl. Phys. **A631**, 70c (1998); R. B. Wiringa, S. C. Pieper, J. Carlson, and V. R. Pandharipande, Phys. Rev. C **62**, 014001 (2000).
- [5] R. F. Bishop, M. F. Flynn, M. C. Boscá, E. Buendía, and R. Guardiola, Phys. Rev. C **42**, 1341 (1990); J. H. Heisenberg and B. Mihaila, *ibid.* **59**, 1440 (1999).
- [6] D. C. Zheng, B. R. Barrett, L. Jaqua, J. P. Vary, and R. L. McCarthy, Phys. Rev. C **48**, 1083 (1993); D. C. Zheng, J. P. Vary, and B. R. Barrett, *ibid.* **50**, 2841 (1994).
- [7] D. C. Zheng, B. R. Barrett, J. P. Vary, W. C. Haxton, and C. L. Song, Phys. Rev. C **52**, 2488 (1995).
- [8] P. Navrátil and B. R. Barrett, Phys. Rev. C **54**, 2986 (1996); **57**, 3119 (1998).
- [9] P. Navrátil and B. R. Barrett, Phys. Rev. C **57**, 562 (1998); **59**, 1906 (1999).
- [10] P. Navrátil, G. P. Kamuntavičius, and B. R. Barrett, Phys. Rev. C **61**, 044001 (2000).
- [11] P. Navrátil, J. P. Vary, and B. R. Barrett, Phys. Rev. Lett. **84**, 5728 (2000).
- [12] A. C. Hayes, Phys. Rep. **315**, 257 (1999).
- [13] P. Vogel, nucl-th/9901027; E. Kolbe, K. Langanke, and P. Vogel, Nucl. Phys. **A562**, 91 (1999).
- [14] M. J. Musolf and T. W. Donnelly, Nucl. Phys. **A546**, 509 (1992).
- [15] M. J. Musolf *et al.*, Phys. Rep. **239**, 1 (1994).
- [16] R. Schiavilla, V. R. Pandharipande, and D. O. Riska, Phys. Rev. C **41**, 309 (1990).
- [17] M. J. Musolf, R. Schiavilla, and T. W. Donnelly, Phys. Rev. C **50**, 2173 (1994).
- [18] S. Karataglidis, P. J. Dortmans, K. Amos, and R. de Swiniarski, Phys. Rev. C **52**, 861 (1995).
- [19] T. Suzuki and H. Sagawa, Nucl. Phys. **A637**, 547 (1998).
- [20] A. C. Hayes and I. S. Towner, Phys. Rev. C **61**, 044603 (2000).
- [21] R. Machleidt, F. Sammarruca, and Y. Song, Phys. Rev. C **53**, 1483 (1996).
- [22] K. Suzuki and S. Y. Lee, Prog. Theor. Phys. **64**, 2091 (1980).
- [23] K. Suzuki, Prog. Theor. Phys. **68**, 246 (1982); K. Suzuki and R. Okamoto, *ibid.* **70**, 439 (1983).
- [24] J. Da Providencia and C. M. Shakin, Ann. Phys. (N.Y.) **30**, 95 (1964).
- [25] K. Suzuki, Prog. Theor. Phys. **68**, 1999 (1982); K. Suzuki and R. Okamoto, *ibid.* **92**, 1045 (1994).
- [26] C. Viazminsky and J. P. Vary, J. Math. Phys. (to be published).
- [27] L. J. Tassie and F. C. Barker, Phys. Rev. **111**, 940 (1958).
- [28] J. P. Vary and D. C. Zheng, *The Many-Fermion-Dynamics Shell-Model Code*, Iowa State University (1994) (unpublished).
- [29] G. F. Bertsch, *The Practioner's Shell Model* (North-Holland, Amsterdam, 1972).
- [30] F. Ajzenberg-Selove, Nucl. Phys. **A506**, 1 (1990).
- [31] I. Tanihata, T. Kobayashi, O. Yamakawa, S. Shimoura, K. Ekuni, K. Sugimoto, N. Takahashi, T. Shimoda, and H. Sato, Phys. Lett. B **206**, 592 (1988).
- [32] A. Nogga, H. Kamada, and W. Glöckle, Phys. Rev. Lett. **85**, 944 (2000).
- [33] S. C. Pieper (private communication).
- [34] R. Pichler, H. Oberhummer, A. Csótó, and S. A. Moszkowski, Nucl. Phys. **A618**, 55 (1997).
- [35] D. DeAngelis, J. R. Calarco, J. E. Wise, H. J. Emrich, R. Neuhausen, and H. Weyand, Phys. Rev. Lett. **70**, 2872 (1993); Phys. Rev. C **52**, 61 (1995).
- [36] W. E. Ormand, Phys. Rev. Lett. **82**, 1101 (1999).
- [37] B. Mueller *et al.*, Phys. Rev. Lett. **78**, 3824 (1997); D. T. Spade *et al.*, **84**, 1106 (2000).
- [38] I. Sick and J. S. McCarthy, Nucl. Phys. **A150**, 631 (1970); A. Nakada, Y. Torizuka, and Y. Horikawa, Phys. Rev. Lett. **27**, 745 (1971); **27**, 1102 (1971); J. A. Jansen, R. Th. Peerdeman, and C. de Vries, Nucl. Phys. **A188**, 337 (1972).